Drops on an arbitrarily wetting substrate: A phase field description

Rodica Borcia,* Ion Dan Borcia, and Michael Bestehorn
Lehrstuhl Statistische Physik, Nichtlineare Dynamik Brandenburgische Technische Universität, Cottbus, Germany
(Received 28 January 2008; published 16 December 2008)

We propose a scheme for studying thin liquid films on a solid substrate using a phase field model. For a van der Waals fluid—far from criticality—the most natural phase field function is the fluid density. The theoretical description is based on the Navier-Stokes equation with extra phase field terms and the continuity equation. In this model free of interface conditions, the contact angle can be controlled through the boundary conditions for the density field at the solid walls [L. M. Pismen and Y. Pomeav, Phys. Rev. E **62**, 2480 (2000)]. We investigate the stability of a thin liquid film on a flat homogeneous solid support with variable wettability. For almost hydrophobic surfaces, the liquid film breaks up and transitions from a flat film to drops occur. Finally, we report on two-dimensional numerical simulations for static liquid drops resting on a flat horizontal solid support and for drops sliding down on inclined substrates under gravity effects.

DOI: 10.1103/PhysRevE.78.066307 PACS number(s): 47.55.D−, 47.54.−r, 68.08.Bc, 68.15.+e

I. INTRODUCTION

Wetting and drying phenomena are a place where chemistry, physics, materials science, and engineering overlap. Plasma treatment or silanization can modify the chemical properties of the solid surface, and hence the surface tensions at solid-vapor and solid-liquid interfaces. These interfacial tensions are responsible for the behavior and properties of commonly used materials such as paints, ink jets, adhesives, detergents, or lubricants. The solid interfacial tension cannot be measured directly. However, measurements can be done indirectly by means of the contact angle of a liquid drop on a solid surface.

The contact angle—the angle between the liquid-vapor interface and the solid support—is specific for any given system and is determined by interactions across the three interfaces. Most often, the concept is illustrated with a small liquid droplet resting in a gas atmosphere on a flat horizontal solid surface (see Fig. 1). The theoretical description of the contact angle arises from the consideration of a thermodynamic equilibrium between the three phases: the liquid phase of the droplet, the solid phase of the substrate, and the gas and/or vapor phase of the ambient. At equilibrium, the chemical potential in the three phases should be equal. It is convenient to frame the discussion in terms of interfacial energies. We denote the solid-vapor interfacial energy as γ_{SV}, the liquid-solid interfacial energy as γ_{LS}, and the liquid-vapor energy (i.e., the surface tension) as γ_{LV}. The shape of the droplet is determined by the Young-Laplace equation which balances the stresses on the contact line [1],

$$\gamma_{SV} - \gamma_{LS} = \gamma_{LV} \cos\,\theta, \tag{1}$$

with θ the contact angle.

There are many ways to characterize contact lines, and particularly moving-line problems. Much effort has been put into studying such problems through asymptotic analysis (see Refs. [2–6], and references therein) and numerical simulations. Numerical simulations for contact line phenomena are mostly based on the sharp interface models [7–9]. In the sharp interface method the interface is tracked by a local moving mesh and has zero thickness. The interface boundary conditions are included into the discrete system of equations at the interface adjacent grid points.

Lattice Boltzmann methods and phase field models provide an alternate description wherein the interface between two fluids is considered to have a nonzero thickness endowed with physical properties such as surface tension. The lattice Boltzmann methods are kinetic methods which compute the system evolution according to a given interparticle potential. The microscopic properties of the system are described by distribution functions which obey the Boltzmann equation with different collision terms. The rules governing the collisions between the particles are designed such that the time averaged motion of the particles is consistent with the Navier-Stokes equation. The phase field models are continuum thermodynamical models. In the phase field method one introduces an order parameter to the usual set of variables to give an explicit indication of the thermodynamic phase in each point of the system. This variable is governed by a partial differential equation over the entire domain and is coupled to velocity, temperature, and concentration fields. For both models the interface is captured implicitly by gradient terms of the density and/or phase field in the free-energy functional of the system. So, the interface does not need to be explicitly tracked. Concerning simulation of dynamic wetting the lattice Boltzmann methods showed considerable success, see Refs. [10,11].

Here, we focus our attention on the phase field model which is the mathematical tool of the present paper. Proposed by Langer in an *ad hoc* manner, the phase field meth-

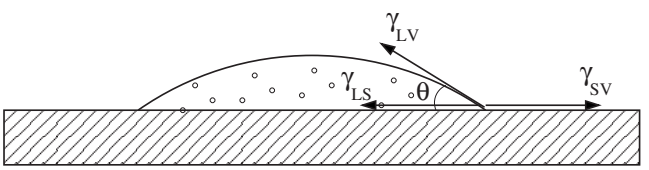

FIG. 1. Balance of stresses at the three-component contact line.

*borcia@physik.tu-cottbus.de

odology has achieved significant importance in modeling solidification phenomena [12–14]. In [15] particular attention is paid to systems described by more complicated order parameters than simple scalars, for example, vectors and tensor fields. The latter are needed to describe phase ordering in nematic liquid crystals. For hydrodynamic systems the phase field models can be simplified using the Cahn-Hilliard equation for incompressible media [15–17] or long-wave approximation for thin films [18]. Thus, for fluid-fluid systems, Bray [15] analyzed the phase separation in binary liquids, Seppecher [16] and Jacqmin [17] investigated moving contact lines for incompressible viscous fluids, and Thiele *et al.* [18] studied sliding drops on slightly sloped planes and small contact angles.

Recently we proposed a phase field model for Marangoni convection in compressible fluids of van der Waals type far from criticality. We chose the fluid density ρ as order parameter. With the help of the phase variable ρ, all the system parameters can be expressed as functions varying continuously from one medium to the other. Therefore, the problem is treated similar to an entire one phase problem and the interface conditions are substituted by some extra terms in the Navier-Stokes equation. The partial differential equation which obeys the phase variable ρ is the continuity equation. The model previously developed for a two-layer geometry [19–22] is extended in this paper to drops and bubbles. Here, the aim is to examine numerically the stability of thin films as well as static and dynamical contact angles.

The outline of the paper is as follows: The phase field model for a two-phase system is briefly depicted in Sec. II. The contact angle description in phase field formulation is given in Sec. III. Section IV investigates the stability of liquid films on a flat solid support with variable wettability and the breakup of an unstable thin liquid film to drops for hydrophobic surfaces. Computer simulations for static liquid drops resting on a flat horizontal solid support and for falling drops on inclined substrates under the gravity effects are presented here. We gather the conclusions in Sec. V.

II. THE FORMALISM

We study a liquid with its own vapor, a situation for which the most natural phase field variable is the density ρ, scaled by the liquid density. So $\rho=1$ designates the liquid phase and $\rho\approx 0$ the vapor bulk. For a two-phase system with diffuse interface and without evaporation phenomena the Helmoltz free-energy functional is given by (see, e.g., Refs. [13,15,19,23,24])

$$\mathcal{F}[\rho] = \int_V \left[f(\rho) + \frac{\mathcal{K}}{2}(\nabla\rho)^2 \right] dV, \tag{2}$$

where the first term in Eq. (2) represents the free-energy density for the homogeneous phases. For a system in equilibrium and without interfacial mass exchange the free-energy density has the form of a double-wall potential with two minima corresponding to the two alternative phases: $\rho=1$ for the liquid and $\rho=0$ for the vapor state. We choose the free-energy density given by

$$f(\rho) = \frac{C}{2}\rho^2(\rho-1)^2. \tag{3}$$

The second term in the free-energy functional (2) is a "gradient energy" which is a function of the local composition. For a flat interface of area ΔA between two coexisting isotropic phases, we obtain the following for the total free-energy $\mathcal{F}(\rho)$ of the system:

$$\mathcal{F} = \Delta A \int_{-\infty}^{+\infty} \left[f(\rho) + \frac{\mathcal{K}}{2}\left(\frac{\partial\rho}{\partial z}\right)^2 \right] dz.$$

The specific interfacial free-energy γ_{LV} (or simply γ) is, by definition, the difference per unit area of interface between the actual free energy of the system and that which it would have if the properties of the phases were continuous throughout. Hence the free-energy excess of the interface takes the form [25]

$$\gamma = \int_{-\infty}^{+\infty} \mathcal{K}\left(\frac{\partial\rho}{\partial z}\right)^2 dz, \tag{4}$$

which gives a direct connection between the surface tension coefficient γ and the gradient energy term $\mathcal{K}(\partial\rho/\partial z)^2/2$.

As already shown in [19] or [20], minimizing the free-energy functional (2), one can derive the nonclassical phase field terms which has to be included in the Navier-Stokes equation for assuring the shear stress balance at the droplet interface

$$\rho\frac{d\vec{v}}{dt} = -\nabla p + \rho\nabla(\nabla\cdot(\mathcal{K}\nabla\rho)) + \nabla\cdot(\eta\nabla\vec{v}) + \nabla(\lambda\nabla\cdot\vec{v}) + \rho\vec{g},$$
$$\lambda \approx \frac{\eta}{3}, \tag{5}$$

with $p=\rho\partial f(\rho)/\partial\rho - f(\rho)$ the thermodynamic pressure. To close the system of equations we need an evolution equation for the phase field. The fluid density ρ obeys the continuity equation

$$\frac{\partial\rho}{\partial t} + \nabla\cdot(\rho\vec{v}) = 0 \tag{6}$$

so that the mass conservation is fulfilled. We solve the problem numerically, starting from an initial noise density

$$\rho(x,z) = a\xi(x,z) + \bar{\rho},$$

where a is the noise intensity, $\xi(x,z)$ is a uniformly random distribution between 0 and 1, and $\bar{\rho}$ was chosen to be zero. A randomly distributed initial density may act as seeds for phase separation in the van der Waals fluid. In the latter, drops or bubbles are found by nucleation and coarsening. The system evolves to drops in a vapor atmosphere or bubbles in a liquid, depending on the total mass (for more details, see [26]). Figure 2 displays two-dimensional (2D) time series in the (x,z) plane for the formation of a liquid drop in a vapor atmosphere for an isothermal system without gravity. The density distributions are represented using gray scale, with white and black for liquid and vapor, respectively.

FIG. 2. Drop formation in a vapor atmosphere under microgravity conditions.

III. CONTACT ANGLE DESCRIPTION IN PHASE FIELD FORMULATION

The boundary conditions for the density field at the solid walls play an important role for the contact angle at the solid surface and determines the position of the droplet. In our model we control the contact angle through the density at the solid boundary ρ_S. Pismen *et al.* assume that for short-ranged solid-fluid interactions compared to the thickness of the diffuse vapor-liquid interface, a supplementary energy term $\gamma_{int}(\rho_S)$ can be locally added in the free-energy functional (2) in the vicinity of the wall. This term is an arbitrary function of ρ_S and describes the fluid-solid interactions. On the other hand, a nonvanishing variation of the density is allowed at the solid boundary $\delta\rho_S$, when the energy functional is varied. Choosing a polynomial function for the dependence of the fluid-solid interaction energy γ_{int} on the fluid density at the solid surface, ρ_S, after some mathematical manipulations, they proved that the only condition enforced on the solid surface is

$$\rho = \rho_S. \tag{7}$$

A flat solid surface with variable wettability can be realized by varying ρ_S in the range $0<\rho_S<1$ (from nonwetting to fully wetting).

Using $\delta\mathcal{F}/\delta\rho=0$, the surface tension coefficient (4) can be expressed as [24]

$$\gamma = \int_{-\infty}^{+\infty} \mathcal{K}\left(\frac{\partial\rho}{\partial z}\right)^2 dz = \int_{\rho_v}^{\rho_l} \sqrt{2\mathcal{K}f(\rho)}d\rho.$$

For the free-energy density (3) and for the partial wetting case $(0<\rho_S<1)$, the interfacial energies γ_{SV}, γ_{LS}, γ_{LV} from (1) become, respectively,

$$\gamma_{SV} = \int_0^{\rho_S} \sqrt{\mathcal{K}C}\rho(1-\rho)d\rho = \frac{\sqrt{\mathcal{K}C}}{6}(1-3\rho_S^2+2\rho_S^3), \tag{8}$$

$$\gamma_{LS} = \int_{\rho_S}^{1} \sqrt{\mathcal{K}C}\rho(1-\rho)d\rho = \frac{\sqrt{\mathcal{K}C}}{6}(3\rho_S^2-2\rho_S^3), \tag{9}$$

$$\gamma_{LV} = \int_0^{1} \sqrt{\mathcal{K}C}\rho(1-\rho)d\rho = \frac{\sqrt{\mathcal{K}C}}{6}. \tag{10}$$

Inserting Eqs. (8)–(10) into the Young-Laplace equation (1), one obtains an analytical relation between the static contact angle and the solid density ρ_S [24],

$$\cos\theta = -1+6\rho_S^2-4\rho_S^3. \tag{11}$$

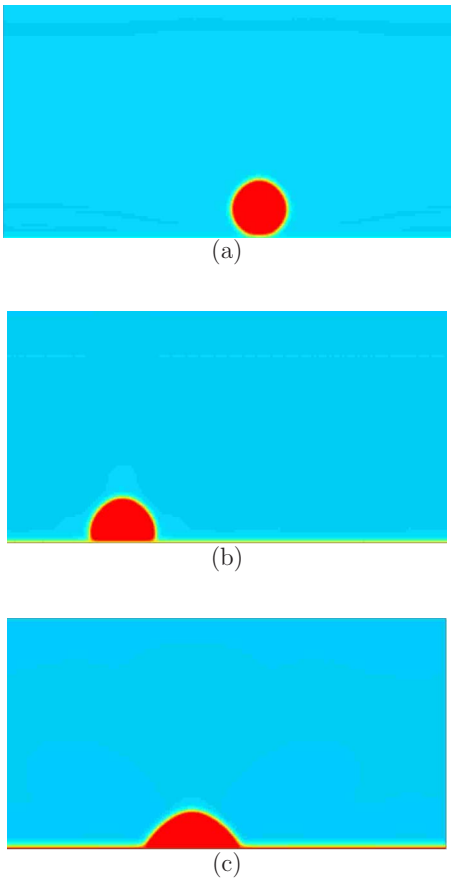

FIG. 3. (Color online) The density field at the solid walls may favor the drop to be in contact with the solid surface: (a) $\rho_S=0.1$; (b) $\rho_S=0.4$; (c) $\rho_S=0.7$.

IV. NUMERICAL SIMULATIONS

We scale the variables by using d, d^2/ν_l, ν_l/d as units for the length, time, and velocity, where $d=\sqrt{\frac{\mathcal{K}}{C}}$ represents the characteristic thickness of the diffuse interface and ν_l is the liquid kinematic viscosity (the index "l" describes the liquid parameters and the index "v" the vapor parameters). The following nondimensional parameters appear: $C_a=\frac{\mathcal{K}}{\rho_l\nu_l^2}$, the capillary number, and $G=\frac{gd^3}{\nu_l^2}$, the Galileo number. For the numerical results presented in this section, $\rho_v/\rho_l\approx10^{-3}$, $C_a=5$, and $G\approx10^{-5}$.

We developed a numerical code in two dimensions based on a finite-difference method with central differences with 400×200 mesh points [27,28]. A similar computational code was earlier developed for 2D phase field models describing floating liquid droplets with applied temperature gradient [26]. The distance between two mesh points is $\Delta x=\Delta z=2$ and the integration time step is $\Delta t=0.05$. The characteristic interface thickness $d=\sqrt{\frac{\mathcal{K}}{C}}$ is smaller than the total thickness of the interface, mostly defined as those corresponding to a fluid density variation from 0.1 to 0.9. (In the diffuse interface one has around seven lattice points.) If the characteristic interface thickness is assumed to be $d\approx1$ nm, the simulations presented below would correspond to a box with 800 nm$\times$400 nm. No-slip conditions for the velocity field are imposed at the wall boundaries ($\vec{v}=0$).

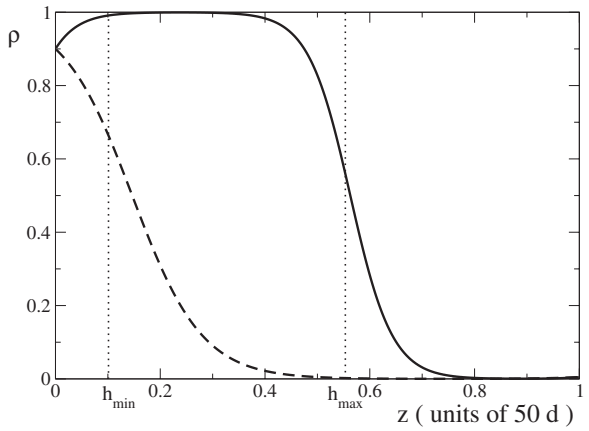

FIG. 4. Two coexisting kink solutions of Eq. (12), corresponding to two different film thicknesses with the same chemical potential. For $\rho_S=0.9$ and $\mu=0$ the two coexisting heights are $h_{min}\approx 5$ and $h_{max}\approx 28$, respectively. The unit d in the z axis label represents a characteristic thickness of the diffuse interface, see the text.

A. Static contact angles

First, we neglect the gravitational force in Eq. (5). For the simulations illustrated in Fig. 2 we imposed $\rho_S=0$ at all four solid boundaries. Here, the liquid drop is pushed away from each wall and after a while a single liquid droplet is obtained in the middle of the box. This is the "no-wetting" case (Lotus effect). Indeed, replacing $\rho_S=0$ in Eq. (11) yields $\theta=180°$, i.e., no-wetting phenomena at the solid boundaries.

In the following we impose periodic lateral boundary conditions. At the top boundary we assume $\rho=0$. At the bottom boundary we consider the solid substrate where $\rho=\rho_S$ (with ρ_S as the control parameter, a number between 0 and 1). For $\rho_S\neq 0$ the drop is attracted to the wall. The boundary conditions now favor the droplet to be in contact with the solid surface (see Fig. 3). The final position of the drop depends on the initial random distribution. The small nuclei, from an early stage of evolution, are in a continuous competition between the coarsening phenomena and the migration to the wall.

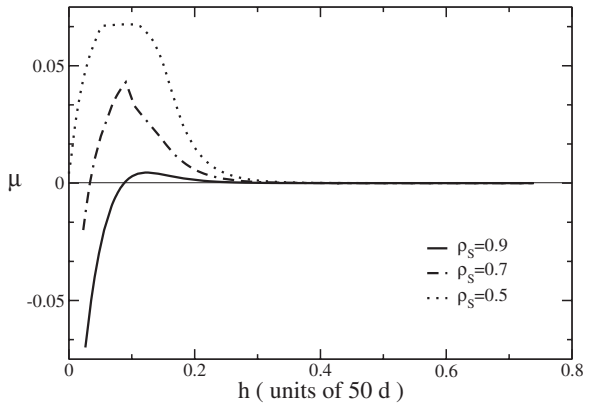

FIG. 5. The chemical potential versus film thickness for different wettability properties of the solid boundary. This plot results from the numerical investigation of Eq. (12) in one dimension under the boundary conditions: $\rho(z=0)=\rho_S$ and $\rho(z\to\infty)=0$ with μ as the free parameter. The axis label unit d represents a characteristic length of the diffuse interface.

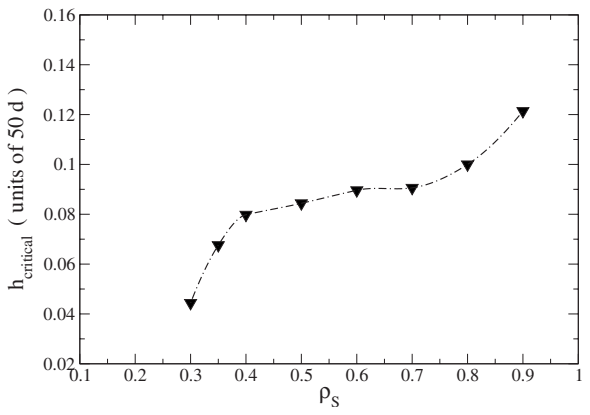

FIG. 6. Location of the maximum of the chemical potential plotted in Fig. 5 for different wettabilities of the solid support. The maximum vanishes at very small ρ_S because one of the kink solutions disappears. For small ρ_S there exists no inflection point on the curve for h_{min} in Fig. 4. The thickness h_{min} of the precursor film cannot be defined. (The axis label unit d represents a characteristic thickness of the diffuse interface.)

The situations illustrated in Fig. 3 correspond to the "partial-wetting" case. Apparent static contact angles were measured using contour plots (level 0.5) of the phase field variable in which tangent lines are drawn at the "macroscopic foot" of the spreading droplet. For $\rho_S=0.1$, the apparent static contact angle measured from Fig. 3(a) is $\theta\approx 161°$. For the same situation the Young-Laplace equation (11) gives $\theta=162°$. For $\rho_S=0.4$ one obtains numerically and analytically the same angle $\theta=107°$. For $\rho_S=0.7$ the static contact angle from Fig. 3(c) is $\theta\approx 52°$ and the relation (11) gives $\theta=55°$. That means an excellent agreement between our phase field simulations and the analytical formula (11).

B. Stability of thin liquid films and the chemical potential

The origin of the predicted wetting behavior can be understood in terms of the dependence of the chemical potential on the film thickness. Pismen and Pomeau [24] studied the Euler-Lagrange equation of Eq. (2) in terms of the chemical potential

$$\mu=\frac{\partial f}{\partial \rho}-\mathcal{K}\frac{\partial^2\rho}{\partial z^2} \tag{12}$$

with only one free parameter determined by the wetting properties of the fluid. They considered a three phase (solid-liquid-gas) contact line and computed the interaction force between the liquid-gas interface and the solid support. It turns out that this force can be repelling (medium and very short distances) or attracting (short and long distances), allowing for two homogeneous and stationary solutions for the film thickness, depicted in Fig. 4 for $\mu=0$ and $\rho_S=0.9$. The dotted lines emphasize the two coexisting heights for the chemical potential $\mu=0$, $h_{min}\approx 5$ and $h_{max}\approx 28$, respectively.

The functional dependence of μ on h as shown in Fig. 5 is analytically derived in [24] for the restricted case $\rho_S=1-\epsilon$, $\epsilon\ll 1$ (corresponding to a hydrophilic wetting surface). Here we shall give numerical solutions of Eq. (12) for any kind of

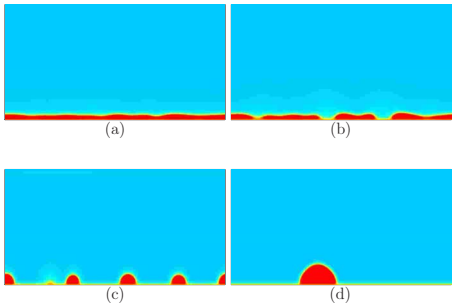

FIG. 7. (Color online) Transitions in a thin unstable liquid layer under microgravity conditions: (a) $t=950$; (b) $t=1400$; (c) $t=2800$; (d) $t=75\,000$ ($h_0=40$, $\rho_S=0.5$).

surface (from no wetting to fully wetting), taking ρ_S as the control parameter of wettability. A plot of the chemical potential for different ρ_S is shown in Fig. 5. To this end, we computed solutions of Eq. (12) which fulfill the boundary conditions $\rho(z=0)=\rho_S$ and $\rho(z\to\infty)=0$. For a given μ, two different solutions are found. One is decreasing monotonically with increasing z, the other increases for small z, reaches a plateau (the liquid phase), and decreases afterwards to zero. As sketched in Fig. 4, the inflection points of $\rho(z)$ define the thicknesses h_{min} and h_{max}. In Fig. 5, in the region where the slope of the chemical potential is negative, the flat film is unstable to arbitrarily small disturbances. The maximum of the curves represented in Fig. 5 is shifted to the left for decreasing ρ_S and vanishes completely for $\rho_S<0.3$ (Fig. 6). This fact reveals that thin liquid films become very unstable on hydrophobic surfaces. If the surface of a flat film is unstable to spatial disturbances, pattern formation sets in, which can be seen in the two-dimensional simulations from the next paragraph (Figs. 7 and 8 from below).

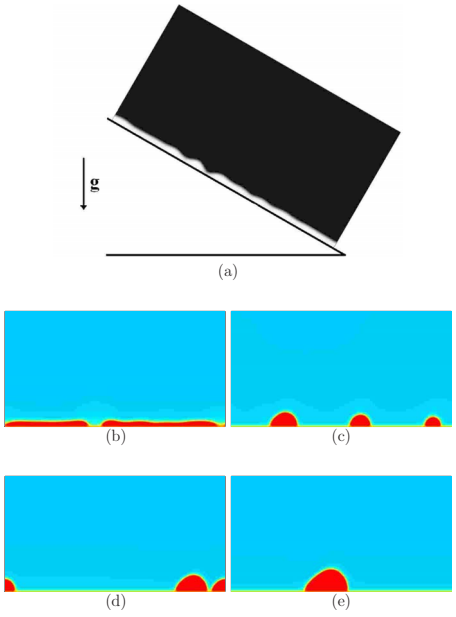

FIG. 8. (Color online) (a) Sketch of a falling liquid film on a sloped plane. (b)–(e) Transitions from a thin flat unstable liquid layer to a drop running down on an inclined substrate under gravity effects: (b) $t=950$; (c) $t=4000$; (d) $t=25\,000$; (e) $t=75\,000$ ($h_0=40$, $\alpha=30°$, $\rho_S=0.5$).

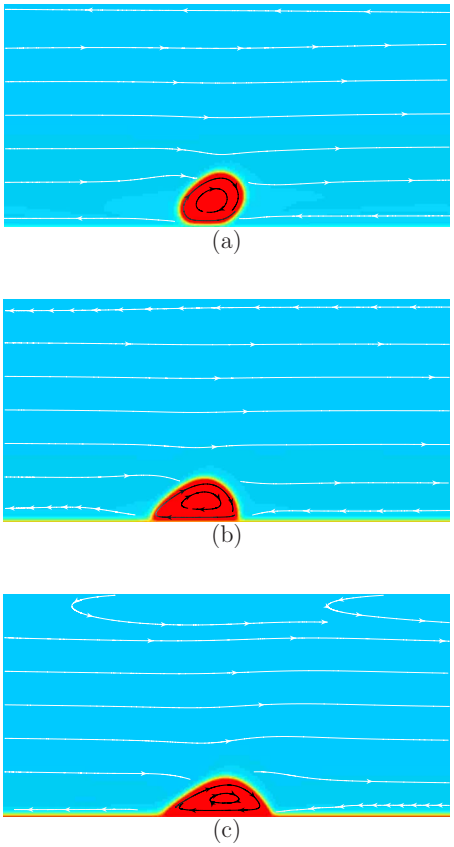

FIG. 9. (Color online) Liquid droplet in its own vapor sliding on a sloped solid surface (from left to right) under gravity effects: (a) $\rho_S=0.1$; (b) $\rho_S=0.5$; (c) $\rho_S=0.7$. Streamlines refer to the system moving with the drop ($h_0=40$, $\alpha=30°$).

C. Dynamic contact angles

Next, we start from an initial flat liquid layer of thickness h_0 described by the density $\bar{\rho}=1$. The flat film is destabilized, adding a small disturbance $a\xi(x,z)$ to the density field with the noise amplitude $a=0.001$. As one can see from Fig. 5, for $\rho_S=0.5$ and $h_0=40$ the thin liquid film is unstable. The liquid film breaks up to produce numerous disconnected droplets, as shown in the Figs. 7 and 8. The snapshots from Fig. 7 corresponds to an initial unstable liquid film (with $h_0=40$, $\rho_S=0.5$) under microgravity conditions and Fig. 8 displays the evolution of the same liquid layer in the presence of gravity effects on an inclined solid support. In both situations, via coarsening, in a late state of evolution only one single drop remains. In Fig. 7 the single remaining drop rests on the substrate, in Fig. 8(e) the drop travels from left to right with constant velocity. For the traveling drop from Fig. 8(e) the scaled drop velocity is $V=0.028$, that means the Reynolds number for our system is around $R_e=V=0.028$.

For a liquid droplet on a sloped solid support, the presence of the tangential component of gravity force leads to different contact angles: the advancing contact angle θ_a in the front of the moving drop and the receding contact angle θ_r in the back (with $\theta_a>\theta_r$). For the same mass in the system

and for the same plane inclination Fig. 9 shows the advancing and receding angles for different wettabilities of the substrate.

In these pictures the streamlines inside and around the drop refer to the comoving frame of reference. The streamline representation emphasizes the self-interaction of the drop. This effect is induced by the lateral periodic boundary conditions. In fact, one considers a chain of drops moving one behind the other at a distance equal to the spatial periodicity. The constant body force per unit volume (the tangential component of gravity force density) parallel to the solid surface together with the boundary conditions imposes a Poiseuille-type flow. As one can observe from Fig. 9, the vapor speed at the top of the droplet acts as a blowing wind in the same direction with the droplet movement. The blowing wind at the top of the droplet induces a rotation motion of the fluid inside the droplet. So, as depicted in Fig. 9 the drop fluid rolls for both hydrophobic and hydrophilic substrates.

V. CONCLUSION

Summarizing, we have investigated film breakup, drop spreading, and drop motion on a flat solid surface with variable wettability using a phase field model. The phase field model previously used for describing Marangoni convection in two-layer systems [19–22] is extended in this paper to drop dynamics on homogeneous substrates. The interactions near a three-phase (solid-liquid-gas) contact line are described using the boundary conditions analytically derived in [24]. The apparent static contact angle numerically computed in this paper is in excellent agreement with the analytical formula (11) given by Pismen *et al.*

For inclined planes our phase field simulations are able to describe advancing and receding contact angles for moving contact lines. The flow motion inside and around the droplet is analyzed. This work is a necessary precursor to understand aspects of interface motions. It allows one to visualize the flow inside a traveling drop, which is very difficult to realize experimentally.

A straightforward but challenging task would be to perform simulations of liquid spreading on a solid support with real properties and to investigate the contact angles on heated substrates, i.e., taking into account the interfacial heat exchange at the liquid-vapor interface and the Marangoni effect, too.

ACKNOWLEDGMENTS

R.B. acknowledges partial financial support from the European Space Agency under Contract No. AO-99-110 CIMEX (Convection and Interfacial Mass Exchange) and I.D.B. acknowledges financial support from Deutsche Forschungsgemeinschaft.

[1] P. G. de Gennes, Rev. Mod. Phys. **57**, 827 (1985).
[2] E. B. Dussan V., J. Fluid Mech. **77**, 665 (1976).
[3] E. B. Dussan V., Annu. Rev. Fluid Mech. **11**, 371 (1979).
[4] A. Novruzi, B. Wetton, and H. Huang, PIMS Report No. PIMS-04-12, 2004 (unpublished).
[5] L. M. Pismen and U. Thiele, Phys. Fluids **18**, 042104 (2006).
[6] V. M. Starov, M. G. Velarde, and C. J. Radke, *Wetting and Spreading Dynamics* (CRC Press Taylor & Francis Group, Boca Raton, 2007).
[7] S. Marella, S. Krishnan, H. Liu, and H. S. Udaykumar, J. Comput. Phys. **210**, 1 (2005).
[8] H. Liu, S. Krishnan, S. Marella, and H. S. Udaykumar, J. Comput. Phys. **210**, 32 (2005).
[9] S. Quan and P. D. Schmidt, J. Comput. Phys. **221**, 761 (2007).
[10] A. R. Davies, J. L. Summers, and M. C. T. Wilson, Int. J. Comput. Fluid Dyn. **20**, 415 (2006).
[11] M. C. T. Wilson, J. L. Summers, Y. D. Shikhmurzaev, A. Clarke, and T. D. Blake, Phys. Rev. E **73**, 041606 (2006).
[12] J. S. Langer, in *Directions in Condensated Matter*, edited by G. Grinstein and G. Mazenko (World Scientific, Singapore, 1986), p. 165.
[13] D. M. Anderson, G. B. McFadden, and A. A. Wheeler, Annu. Rev. Fluid Mech. **30**, 139 (1998).
[14] D. M. Anderson, G. B. McFadden, and A. A. Wheeler, Physica D **135**, 175 (2000).
[15] A. J. Bray, Adv. Phys. **43**, 357 (1994).
[16] P. Seppecher, Int. J. Eng. Sci. **34**, 977 (1996).
[17] D. Jacqmin, J. Fluid Mech. **402**, 57 (1999).
[18] U. Thiele, M. G. Velarde, K. Neuffer, M. Bestehorn, and Y. Pomeau, Phys. Rev. E **64**, 061601 (2001).
[19] R. Borcia and M. Bestehorn, Phys. Rev. E **67**, 066307 (2003).
[20] R. Borcia, D. Merkt, and M. Bestehorn, Int. J. Bifurcation Chaos Appl. Sci. Eng. **14**, 4105 (2004).
[21] R. Borcia and M. Bestehorn, Eur. Phys. J. B **44**, 101 (2005).
[22] R. Borcia and M. Bestehorn, Int. J. Bifurcation Chaos Appl. Sci. Eng. **16**, 2705 (2006).
[23] D. Jasnow and J. Viñals, Phys. Fluids **8**, 660 (1996).
[24] L. M. Pismen and Y. Pomeau, Phys. Rev. E **62**, 2480 (2000).
[25] J. W. Cahn and J. E. Hilliard, J. Chem. Phys. **28**, 258 (1958).
[26] R. Borcia and M. Bestehorn, Phys. Rev. E **75**, 056309 (2007).
[27] C. Hirsch, *Numerical Computation of Internal and External Flows* (Wiley, New York, 1998), Vol. 1, p. 201.
[28] M. Bestehorn, *Hydrodynamik und Strukturbildung* (Springer-Verlag, Berlin, 2006), p. 347.